Constraints on $f(R)$ and normal-branch Dvali-Gabadadze-Porrati modified gravity model parameters with cluster abundances and galaxy clustering

Rayne Liu,[1,*] Georgios Valogiannis,[2,*] Nicholas Battaglia,[1] and Rachel Bean[1]
[1]*Department of Astronomy, Cornell University, Ithaca, New York 14853, USA*
[2]*Department of Physics, Harvard University, Cambridge, Massachusetts 02138, USA*

(Received 29 January 2021; accepted 4 October 2021; published 18 November 2021)

We present forecasted cosmological constraints from combined measurements of galaxy cluster abundances from the Simons Observatory and galaxy clustering from a DESI-like experiment on two well-studied modified gravity models, the chameleon-screened Hu-Sawicki $f(R)$ model and the nDGP braneworld Vainshtein model. A Fisher analysis is conducted using σ_8 constraints derived from thermal Sunyaev-Zel'dovich (tSZ) selected galaxy clusters as well as linear and quasilinear redshift-space 2-point galaxy correlation functions. We find that the cluster abundances drive the constraints on the nDGP model while $f(R)$ constraints are led by galaxy clustering. The two tracers of the cosmological gravitational field are found to be complementary, and their combination significantly improves constraints on the $f(R)$ in particular in comparison to each individual tracer alone. For a model of $f(R)$ with a general relativity (GR) fiducial case ($f_{R0} = 0$), we find a 2-σ upper limit of $f_{R0} \leq 5.68 \times 10^{-7}$. For the well-studied log-based fiducial parameter value in $f(R)$, $\log_{10}(f_{R0}) = -5$, paired with the parameter value $n = 1$, we find combined 1-σ constraints of $\sigma(\log_{10}(f_{R0})) = 0.12$ and $\sigma(n) = 0.36$. For the nDGP model with fiducial $n_{\mathrm{nDGP}} = 1$ we find $\sigma(n_{\mathrm{nDGP}}) = 0.087$. Our results present the exciting potential to utilize upcoming galaxy and CMB survey data available in the near future to discern and/or constrain cosmic deviations from GR.

DOI: 10.1103/PhysRevD.104.103519

I. INTRODUCTION

The ΛCDM model accredits the acceleration of cosmic expansion [1–9] to the negative pressure exerted by an unknown dark energy, either as a cosmological constant Λ with a canonical equation of state $w = -1$, or as a variable scalar field known as quintessence [10–12]. However, more direct evidence for of the underlying nature of dark energy remains absent. The cosmological constant explanation suffers from stark incompatibility since the value inferred from astronomical observations is ∼120 orders of magnitude smaller than that predicted in particle physics; the quintessence field theories attempting to resolve the discrepancy face subsequent fine-tuning problems [13].

Modified gravity (MG) theories attempt to avoid this extra energy component by explaining the accelerating Universe with altering the standard theory of gravity, namely Einstein's general relativity (GR), in large scales [14–16]. While GR has been meticulously tested with astrophysics on smaller scales, such as the Solar System tests [17] and strong-gravity tests via gravitational waves [18,19], MG can potentially be applicable to larger cosmic scales with relatively weak gravitational fields. Nevertheless, such remarkable tests of GR on small scales have already imposed stringent constraints [20–25], leaving a limited parameter space for most MG models. Two particularly well-studied MG models that survive are the Hu-Sawicki $f(R)$ model series [26], which feature a Chameleon mechanism, and the normal-branch Dvali-Gabadadze-Porrati braneworld model (nDGP) [27], which introduces a fifth dimensional force (Vainshtein mechanism). They successfully evade the above small-scale tests, while also reproducing an expansion history indistinguishable from ΛCDM. Hence, constraints via other independent observational quantities, especially the growth of the cosmic large-scale structure (LSS), are of crucial importance [28]. Complementary to constraints via geometric distance measurements of the expansion history, LSS growth are very sensitive to the phenomenology of the cosmological MG models of interest [28–30].

Current and future LSS surveys will measure the abundance of galaxy clusters, as well as the three-dimensional positions and velocities of galaxy halos. Such measurements are powerful probes of the LSS growth and clustering, and subsequently the nature of gravity and dark energy. In this work, we explore the constraining power of cluster abundances from upcoming observations of the thermal Sunyaev-Zel'dovich (tSZ) effect by the Simons Observatory [31] and galaxy clustering from spectroscopic observations by the Dark Energy Spectroscopic Instrument

*R. L. and G. V. contributed equally to the work.

(DESI) [32],[1] both when considered independently and combined with each other.

Galaxy clusters have long been regarded as a promising set of observables to test MG, and their abundances represented as number counts, as well as mass profiles, both serve as powerful tools. Potential constraints on MG using a wide variety of signal types have been considered, including x rays [33–36], the tSZ effect [34,37–39], and weak lensing [40,41]. In this work, the constraints from abundances of galaxy clusters over the large linear scales is inferred through constraints on measurements of σ_8, the mean amplitude of matter energy density fluctuations. We base these constraints on the forecasted weak-lensing and CMB-halo lensing calibrated tSZ galaxy cluster abundances in [39,40].

Meanwhile, mapping out the three-dimensional clustering of galaxies across the cosmic history offers another window into the underlying physical processes, including the gravity models, that shaped the LSS. Building upon the legacy of the recently completed analysis by the extended baryon oscillation spectroscopic survey (eBOSS) [42–44], DESI is expected to constrain the properties of gravity and dark energy at unprecedented levels of accuracy [45], in combination also with the next generation of cosmological surveys, such as Euclid [46], the Vera C. Rubin Observatory Legacy Survey of Space and Time (LSST) [47,48], the Nancy Grace Roman Space Telescope [7] and SPHEREx [49]. A necessary requirement for the optimal interpretation of this upcoming wealth of observational data is the ability to reliably model the clustering statistics in the variety of competing scenarios, in our case the landscape of MG models. When galaxies are identified through spectroscopic measurements, in particular, one needs to take into account not only the nonlinear growth of structure, but also the fact that galaxy peculiar velocities induce an observed anisotropy in the clustering pattern, the redshift-space distortions (RSD) [50–52]. In this study we capture these effects closely following the recent work of [53], that employed the Gaussian streaming model (GSM) approach [54–56] with Lagrangian perturbation theory [57–65] in the context of MG [66–68], in order to successfully model the multipoles of the anisotropic correlation function of halos in theories beyond GR.

We forecast individual and joint constraints on MG from these two probes using Fisher analysis. In addition to obtaining model-dependent constraints through a state-of-the-art treatment of the galaxy bias and RSD effects in MG, this work explores tests of gravity through the combination of these two complementary and promising probes of the LSS. Our paper is structured as follows: first, in Sec. II, we outline our theoretical and observational formalism and assumptions. We then present our analysis results in Sec. III, with a subsequent discussion including implications for future work in Sec. IV. The details of the particular model used to obtain the galaxy clustering covariance matrices are presented in the Appendix.

[1] https://www.desi.lbl.gov/

II. FORMALISM

A. Modified gravity models

We focus on two quintessential models in the literature of MG, the Hu-Sawicki $f(R)$ and the nDGP braneworld models, which respectively realize the Chameleon and Vainshtein classes of screening.

1. $f(R)$ Hu-Sawicki model

In the Hu-Sawicki $f(R)$ model, a nonlinear modification function, $f(R)$, of the Ricci scalar is added to the standard Einstein-Hilbert action,

$$S = \int d^4x\sqrt{-g}\left[\frac{R + f(R)}{16\pi G} + \mathcal{L}_m\right], \tag{1}$$

where G is the Newtonian gravitational constant, $\mathcal{L}_m$ the matter Lagrangian, and $f(R)$ induces the accelerating Universe instead of a cosmological constant Λ. Through a conformal transformation, (1) as the Einstein frame expression can be cast into the form of a scalar-tensor theory with the scalaron, $f_R \equiv \frac{df(R)}{dR}$, acting as the MG-induced degree of freedom [69]. Imposing an expansion history identical to ΛCDM in the high curvature limit, a present day value of the scalaron can be obtained as [53]

$$f_{R0} = -n\frac{c_1}{c_2^2}\left[\frac{\Omega_{m0}}{3(\Omega_{m0} + \Omega_{\Lambda 0})}\right]^{n+1}, \tag{2}$$

where Ω_{m0} and $\Omega_{\Lambda 0}$ are the normalized density parameters for nonrelativistic mass and dark energy today; they, as ΛCDM parameters, appeared in (2) as a result of our assumption on the expansion history. Instead of using c_1/c_2^2 as the free parameter in (2), the pair of f_{R0} (typically $|f_{R0}|$ in the literature, and for the rest of this paper we only consider $f_{R0} \geq 0$) and n are commonly used. We recover the ΛCDM (GR) model when $f_{R0} \to 0$, which is the case in regions of high Newtonian potential, where the chameleon field becomes very massive due to the effect of the screening mechanism [70,71].

Extensive studies of the Hu-Sawicki model in the past decade have tightened constraints on the available parameter space of the model [72,73] but have still left the model observationally viable and theoretically attractive, as it is devoid of instabilities [74]. For these reasons, it serves as the ideal test bed for us to explore constraints on MG with upcoming surveys of the LSS and CMB.

2. nDGP model

The Dvali-Gabadadze-Porrati (DGP) model is a representative example of the Vainshtein screening mechanism [75,76] and features a modification to gravity due to a large extra fifth dimension of spacetime. The modified Einstein-Hilbert action is in this case,

$$S = \int d^4x\sqrt{-g}\left[\frac{R}{16\pi G} + \mathcal{L}_m\right] + \int d^5x\sqrt{-g_5}\frac{R_5}{16\pi G r_c}, \tag{3}$$

where R_5 and g_5 denote respectively the corresponding Ricci scalar and metric determinant of the fifth dimension, and r_c the crossover distance, a characteristic scale below which GR model becomes four dimensional. A more appealing self-accelerating DGP model branch (sDGP), which requires no dark energy, has been shown to suffer from undesirable instabilities [77]; hence we study the "normal" branch (nDGP) coupled with a dark energy component to match the desired ΛCDM expansion history, which still remains interesting due to prior simulation investments. In this case, the only free parameter to constrain is $n = H_0 r_c$ (H_0 being the Hubble constant), of which the extensively studied values are 1 and 5. GR is recovered when $n \to \infty$, corresponding to the presence of large gradients of gravitational forces in Vainshtein screening.

B. Cluster abundances and σ_8

The constraints by cluster abundances are modeled after results obtained from [40], in which a Fisher forecast based on tSZ-selected galaxy clusters from a CMB-S4-like experiment is extended to model-independent constraints on the time-evolution of $\sigma_8(z)$. Specifically, we use forecasted errors on $\sigma_8(z)$ from [40], which predicted tSZ cluster abundances for Simons Observatory and included mass calibrations from optical weak-lensing and CMB-halo lensing while marginalizing over ΛCDM and seven cluster mass-observable scaling relation parameters [for more details see 40]. The correlations between these mass-observable scaling relation and cosmological parameters are shown in Fig. 6 of [40]. σ_8 is the amplitude of matter energy density fluctuations smoothed out over a scale of 8 Mpc/h, and its evolution over redshift z is a promising probe of structure growth in the linear density perturbation regime.

To predict $\sigma_8(z)$ from MG models, we calculate σ_R through the standard deviation of the probability density function of the matter density fluctuations, convoluted with a spherical top-hat window function $W(\mathbf{r}, R)$ with radius R,

$$W(\mathbf{r}, R) = \frac{1}{4\pi R^3/3} = \begin{cases} 1, & |\mathbf{r}| \le R, \\ 0, & |\mathbf{r}| > R. \end{cases} \tag{4}$$

Fourier transforming, Parseval's theorem gives

$$\sigma_R{}^2(z) = \int_0^\infty \frac{P(k,z)}{2\pi^2}\left[\frac{3j_1(kR)}{kR}\right]^2 k^2 dk, \tag{5}$$

where $P(k,z)$ is the matter power spectrum at wave number k and redshift z, $j_1(kR)$ is the spherical Bessel function of the first kind, and $3j_1(kR)/(kR)$ is the Fourier transform of the window function. 8 Mpc/h is then assigned to R.

In general, the power spectrum in MG can be obtained from the ΛCDM one by considering the modifications to the linear growth factor $D(k,z)$,

$$P_{\rm MG}(k,z) = P_{\Lambda\rm CDM}(k, z=0)\cdot\left(\frac{D_{\rm MG}(k,z)}{D_{\Lambda\rm CDM}(z=0)}\right)^2. \tag{6}$$

The growth factors, more commonly expressed as $D(k,a)$ [$a = 1/(1+z)$ being the scale-factor], are obtained by solving the modified linear density evolution equations, extracted from the work of [78],

$$\ddot{D} + 2H\dot{D} - 4\pi G\rho_m(1+g_{\rm eff})D = 0, \tag{7}$$

where H is the Hubble parameter, ρ_m is the nonrelativistic matter density, and dots are derivatives with respect to time t. The effective gravitational factor $g_{\rm eff}$ for $f(R)$ [79] is

$$g_{\rm eff} = \frac{k^2}{3(k^2 + a^2 m(a))^2}, \tag{8}$$

with the associated mass term,

$$m(a) = \frac{1}{c}\sqrt{\frac{[\Omega_{m0} + 4(1-\Omega_{m0})]^{-(n+1)}}{(n+1)|f_{R0}|}} \times \sqrt{\left[\frac{\Omega_{m0}}{a^3} + 4(1-\Omega_{m0})\right]^{n+2}}, \tag{9}$$

and for nDGP,

$$g_{\rm eff} = \frac{1}{3\beta(a)}, \tag{10}$$

where

$$\beta(a) = 1 + 2Hr_c\left(1 + \frac{\dot{H}}{3H^2}\right) = 1 + 2\frac{H}{H_0}n\left(1 + \frac{\dot{H}}{3H^2}\right). \tag{11}$$

For more direct comparison with the standard ΛCDM model, we evaluate $\sigma_{8(\rm MG)}/\sigma_{8(\Lambda\rm CDM)}$. We obtain the ΛCDM linear matter power spectrum at $z = 0$, $P_{\Lambda\rm CDM}(k, z=0)$, from the Boltzmann code CAMB [80–82] as a starting point, and then utilize (5) and (6) to determine $\sigma_{8(\rm MG)}/\sigma_{8(\Lambda\rm CDM)}$. Based on the assumptions in MG, the structure growth at early times should be indistinguishable from that in ΛCDM;

hence we normalize the ratio to 1 at redshift $z = 10$, high enough to set the initial conditions of structure growth. We note that the growth factors between the GR limit solution of (7) and the ΛCDM prediction from CAMB differ at the level far below the statistical uncertainties to affect the results of the Fisher analysis, and are corrected by normalization using the former.

Our solution of $D(k, z)$ [or $D(k, a)$] for the $f(R)$ model is checked against the work of [83] in which the code for linear perturbation in MG is slightly modified for our purpose. For both the ΛCDM and the nDGP models, the growth factor $D(z)$ [or $D(a)$] are scale-independent and are checked against the empirical fitting function proposed by [29]

$$g(a) \equiv D(a)/a = \exp\left[\int_0^a \frac{da'}{a'}[\Omega_m(a')^\gamma - 1]\right], \quad (12)$$

where $\Omega_m(a) = \Omega_{m0} a^{-3}/(H/H_0)^2$, γ is taken as 0.55 for ΛCDM, and 0.68 for both sDGP and nDGP with a modified expansion history [29]. This agreement remains stable when Ω_{m0} is varied in a small range around our fiducial value $\Omega_{m0} \sim 0.315$. In our work after the check, the ΛCDM expansion history (Hubble parameter) is imposed on the nDGP model.

Using the marginalized errors on $\sigma_8(z)$ to summarize the constraints from cluster abundances has the following advantages. There is not much information lost since we are examining the linear regime, despite the fact that the constraints are compressed into a root-mean-squared quantity as σ_8. Performing a Fisher analysis using σ_8 based on [40] is not only faster but also more conservative in the sense that it does not introduce extra degeneracy breaking as is the case for full Fisher analyses where ΛCDM and nuisance parameters are not already marginalized over.

C. Galaxy clustering correlations

The LSS of the Universe, as traced by the observed inhomogeneous clustering pattern of galaxies, has been formed by the nonlinear gravitational collapse of the primordial density distribution. We can model the observed clustering statistics of galaxies in MG, by taking into account the crucial effects of clustering in the quasilinear regime, large-scale galaxy bias and redshift space distortions (RSD). Our modeling procedure summarized below is tailored to DESI observations and is heavily based upon the previous works of [53,68].

In the intermediate, quasilinear scales, higher order perturbation theory can substantially improve upon the accuracy of the simple linear treatment, allowing for a robust modeling of the clustering statistics, without the need to resort to computationally expensive N-body simulations. In this work we focus on the Lagrangian perturbation theory (LPT), in which the expansion parameter is a vector field, $\mathbf{\Psi}$, which displaces each fluid particle from its initial position, $\mathbf{q}$, to its final, Eulerian one, $\mathbf{x}(\mathbf{q}, t)$, through the mapping,

$$\mathbf{x}(\mathbf{q}, t) = \mathbf{q} + \mathbf{\Psi}(\mathbf{q}, t). \quad (13)$$

The first order LPT solution is the famous Zel'dovich approximation [57]. In MG theories, an additional degree of freedom is present, altering the perturbed Einstein equations and the nonlinear gravitational evolution of dark matter overdensities, and subsequently the framework of LPT, as detailed in [66–68,84].

The galaxies observed by surveys of the LSS do not perfectly trace the underlying dark matter density distribution, but rather are biased tracers of it [85]. In the simpler picture of linear perturbation theory, the large-scale overdensity of biased tracers (i.e., galaxies) is proportional to the underlying dark matter overdensity [86], while a wide range of more sophisticated treatments have been developed in the literature [87]. When working in Lagrangian space as is in this work, biased tracers are identified as regions of the primordial density field preselected by a biasing function, F, that depends on the local matter density [63,64]. Given the statistical nature of cosmic density fields, the simplest meaningful observable statistic (in the configuration space) is the two-point correlation function, $\xi_X(r)$, of tracers correlated over a distance r,

$$\xi_X(r) := \langle \delta_X(\mathbf{x}) \delta_X(\mathbf{x} + \mathbf{r}) \rangle, \quad (14)$$

where the angle brackets denote an ensemble average. In Lagrangian space, the "convolution Lagrangian perturbation theory" (CLPT) [64,88,89] was shown to work particularly well at recovering the correlation function of halos from N-body simulations, in ΛCDM cosmologies. Building upon these works, [67,68] then expanded CLPT in the case of MG theories and successfully recovered the real-space two-point correlation function of dark matter haloes across the parameter space of the $f(R)$ and nDGP MG scenarios.

In addition to imperfectly tracing the dark matter distribution of the cosmic web, galaxies identified through spectroscopic means are observed in redshift space, rather than in real space, which further distorts the observed clustering pattern, known as the redshift space distortions (RSD) [50–52]. Due to its peculiar velocity about the Hubble flow, $\mathbf{v}(\mathbf{x})$, a galaxy with real space position $\mathbf{x}$ will be instead observed at a redshift space position,

$$\mathbf{s} = \mathbf{x} + \frac{\hat{z} \cdot \mathbf{v}(\mathbf{x})}{aH(a)} \hat{z}, \quad (15)$$

with $H(a)$ the Hubble parameter evaluated at scale-factor a. As a consequence, the redshift-space 2-point correlation function for biased tracers,

$$\xi_X^s(\mathbf{r}) = \langle \delta_X(\mathbf{s})\delta_X(\mathbf{s}+\mathbf{r})\rangle, \tag{16}$$

becomes directionally dependent, unlike the real-space expression (14). In large linear scales, coherent infall leads to the "Kaiser boost," an enhancement on the amplitude of the two-point correlation function, whereas in the nonlinear scales, the random velocities within virialized structures lead to the "Fingers-of-God" (FOG) suppression effect.

The Gaussian streaming model (GSM) [54–56] has been shown to be very successful in modeling the anisotropic RSD correlation function of halos, through a convolution of the halo real space correlation function with the probability velocity distribution of tracers, that is approximated as a Gaussian [90]. In particular, given the real-space mean pairwise velocity along the pair separation vector of a pair of tracers, $v_{12}(r)$, as well as its pairwise velocity dispersion, $\sigma_{12}^2(r)$, the GSM gives the expression for the anisotropic RSD correlation function,

$$1+\xi_X^s(s_\perp, s_\parallel) = \int_{-\infty}^{\infty} \frac{dy}{\sqrt{2\pi\sigma_{12}^2(\mathbf{r})}}[1+\xi_X^r(r)] \times \exp\left[-\frac{(s_\parallel - y - \mu v_{12}(r))^2}{2\sigma_{12}^2(\mathbf{r})}\right], \tag{17}$$

where $s_\perp$, $s_\parallel$ are the perpendicular and parallel to the line-of-sight components of the redshift-space separation s, with $s=\sqrt{s_\perp^2+s_\parallel^2}$, $r=\sqrt{s_\perp^2+y^2}$ and $\mu=\hat{r}\cdot\hat{z}=\frac{y}{r}$. Using CLPT to model the three ingredients that enter the prescription (17), $\xi_X^r(r)$, $v_{12}(r)$, $\sigma_{12}^2(\mathbf{r})$, and based on the MG implementations of [67,68], [53] was able to successfully model the simulated RSD correlation function of haloes in the $f(R)$ and nDGP gravity scenarios up to 1-loop order in PT. For the purposes of this work, we only use the first order LPT solution (Zel'dovich approximation [57]) to evaluate the GSM ingredients, mainly because our model for the evaluation of the clustering covariance matrix does not incorporate non-Gaussian corrections, as we explain in the Appendix.

In addition to the LPT growth factors and the linear power spectrum, derived from the underlying cosmological model, we include two nuisance parameters in the modeling of the observed galaxy clustering correlation function using the CLPT and GSM framework laid out in this section.

The first nuisance parameter sets the first-order Lagrangian bias parameter, $b_1^E(z)$, which we use to calculate the Lagrangian bias up to second order (for a one-loop prediction). We assume a redshift evolution for the bias of the form $b_1^E(z)D(z) = \text{constant}$, following [91], where $D(z)$, the linear growth factor under ΛCDM, is normalized to unity at $z=0$. In our analysis, we treat $b_1^E(z=0)$ as a nuisance parameter over which we marginalize separately for the two types of DESI-like galaxy samples, luminous red galaxies (LRGs) and the emission line galaxies (ELGs), with fiducial values of $b_1^E(z=0)=1.7$ and 0.84 respectively.

We do not treat the second order bias parameter, b_2^E, as a nuisance parameter in its own right, but rather determine it in terms of the $b_1^E(z)$ prediction through the fitting formula calibrated from N-body simulations [92],

$$b_2^E = 0.412 - 2.143 b_1^E + 0.929(b_1^E)^2 + 0.008(b_1^E)^3. \tag{18}$$

Fixing b_2, rather than allowing it to vary independently, is motivated by previous work [93], in which the galaxy correlation function multipoles on the large scales on which we are focusing were found to be insensitive to the particular values of the higher order bias factors ($b_n \geq b_2$), which were fixed to the corresponding peak-background split (PBS) prediction. This fact was further confirmed in the context of MG models in [53], with the only difference being that in the current work we use the improved empirical fit from Eq. (18) to determine b_2, instead of the PBS prediction.

Finally, the Eulerian bias values b_1^E and b_2^E can be converted to their Lagrangian space equivalents through the known conversion relationships [94,95],

$$b_1^L = b_1^E - 1,$$
$$b_2^L = b_2^E - \frac{8}{21} b_1^L. \tag{19}$$

Motivated by the findings in [53], we only include the b_1 and b_2 bias terms (together with the FoG contribution) as these were shown to be sufficient to accurately capture the RSD correlation function from the N-body simulations for the MG models we consider. Further, since we focus on the linear and quasilinear regimes, using the Zel'dovich approximation, we do not attempt to include the small-scale effects through the corresponding EFT corrections, as was done e.g., in [96] for GR and more recently [97] for MG theories, but rather reserve these expansions for future work. We finally note that throughout this analysis the bias is taken to be scale-independent, a good approximation for our scales of interest, as was explained in [53] and also previously confirmed by simulations in [98], for both GR and MG.

The second nuisance parameter we include is a constant offset, α_σ, that needs to be added to the modeled galaxy pairwise velocity dispersion,

$$\sigma_{12}^2 \to \sigma_{12}^2 + \alpha_\sigma, \tag{20}$$

such that the latter matches the observed prediction from simulations/observations at the large scale limit, as we found in [53]. This correction aims to capture unknown small-scale nonlinear effects and is essentially the equivalent of the "Fingers-of-God" free parameter, $\sigma_{\rm FoG}^2$, that is

commonly employed in the simple phenomenological dispersion models [99,100]. While, in principle, the free parameter α_σ is different for each of the two galaxy samples we consider, in [53] it is shown that in the Zel'dovich regime, which we adopt in this work, the best-fit value of α_σ changes only by a very small amount across the range of MG models and halo mass ranges we examine. This motivates the use of a common fiducial value for both the ELG and the LRG galaxy samples, in all cases.

All of those ingredients are combined to produce a prediction, by means of Eq. (17), for the MG RSD galaxy correlation function for the ELG and the LRG DESI galaxy samples at a given redshift z. As commonly performed in the literature, we further decompose the correlation function through a multipole expansion in a basis of Legendre polynomials, $L_l(\mu_s)$,

$$\xi(s,\mu_s) = \sum_l \xi_l(s) L_l(\mu_s), \tag{21}$$

where the multipoles of order l are given by

$$\xi_l(s) = \frac{2l+1}{2}\int_{-1}^{1} d\mu_s \xi(s,\mu_s) L_l(\mu_s), \tag{22}$$

with $\mu_s = \hat{z}\cdot\hat{s} = s_\parallel/s$. We restrict our analysis on values $l = \{0,2,4\}$, which correspond to the monopole, the quadrupole and the hexadecapole, respectively (first three nonvanishing multipoles). In Fig. 1 we demonstrate an example of how the correlation function multipoles deviate from the corresponding ΛCDM prediction for the ELG sample at $z = 0.05$, in the $f(R)$ scenario, for two sets of f_{R0} and n values. For a more thorough discussion of this topic, we refer the reader to [53,67,68].

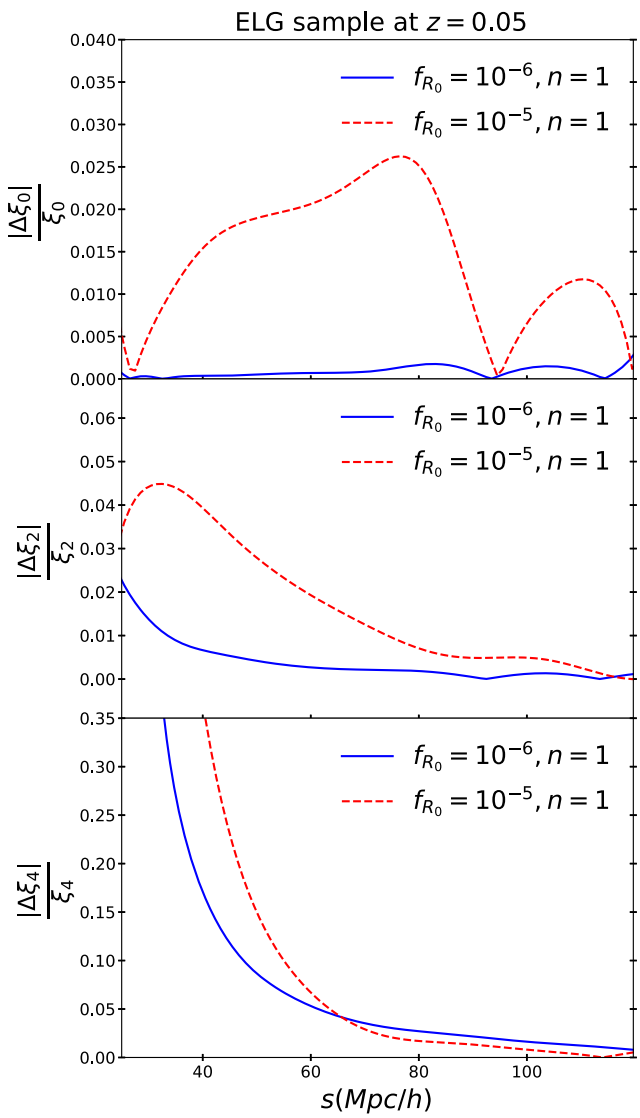

FIG. 1. The fractional deviations of the monopole [top], quadrupole [middle] and hexadecapole [bottom] of the anisotropic correlation function in the $f_{R0} = 10^{-5}$ [red dashed] and $f_{R0} = 10^{-6}$ [solid blue] $f(R)$ scenarios with respect to the corresponding ΛCDM prediction for the ELG sample at $z = 0.05$.

D. Fisher analysis

For the forecasted constraints on the two MG models we use Fisher analyses on the tracers of the LSS, e.g., cluster abundances in the linear regime and galaxy clustering in the quasilinear regime. Our adopted fiducial background cosmology and MG parameters are shown in Table I, following [40]. We consider three different $f(R)$ scenarios with fiducial values $f_{R0} = 0$ (referred to as "near-GR"), 10^{-5} ("F5"), and 10^{-6} ("F6"). In the near-GR case at $f_{R0} = 0$, the parameter n is not well-defined and has no impact on the growth, so we consider its value as fixed at $n = 1$ and do not include it as a Fisher parameter. Furthermore, we consider two nDGP scenarios with fiducial parameter

TABLE I. The fiducial cosmological parameters for the background cosmology considered in the analysis (denoted as ΛCDM) and the baseline $f(R)$ and nDGP MG scenarios. We add that the nuisance parameters refer only to the galaxy clustering evaluation.

	Parameter	Fiducial value(s)
ΛCDM	$\Omega_c h^2$	0.1194
	$\Omega_b h^2$	0.022
	H_0	67.0
	$10^9 A_s$	2.2
	n_s	0.96
$f(R)$	f_{R0}	0, 10^{-5}, 10^{-6}
	n	1
nDGP	$n_{\rm nDGP}$	1,5
Nuisance	$b_1^E(z=0)$	1.7 (LRG) 0.84 (ELG)
Parameters	α_σ (in Mpc/h)	0.5

values $n = \{1, 5\}$, that we respectively refer to as N1 and N5.

To obtain constraints on f_{R0}, we use two different parameter space configurations. For the near-GR fiducial model, we use a linear parameter space, recognizing that we are probing a direct and comparatively small deviation from GR. Such a linear prior is used in the literature, see for example, Fig. 18 in [101], where ω_{BD}^{-1} is a generalized equivalent of f_{R0}. For F5 and F6 cases; on the other hand, we use a logarithmic prior, i.e., the corresponding parameter we use to constrain the models is $\log_{10}(f_{R0})$. This is a common choice for constraining power-law-like parameters representing further deviations from GR; see [83,102] for example.

In theory, the constraints from the two prior configurations are relatable through a direct transformation from the chain rule: $\sigma[f_{R0}] = \sigma[\log_{10}(f_{R0})] \cdot [f_{R0} \ln(10)]$. Problems might arise on the lower limits of the constraints after such a transformation, which might reach down beyond the physically allowed range of $f_{R0} \geq 0$. Regarding this, we note that for each Fisher analysis, a Gaussian distribution is assumed of the likelihood around the fiducial value, i.e., a Gaussian distribution in the linear space around f_{R0} for the near-GR case, and likewise in the log space around $\log_{10}(f_{R0})$ for F5 and F6. A Gaussian distribution of constraints in the log space implies a skewed distribution of constraints linearly and vice versa. In order to keep our assumptions self-consistent, and supported by the literature as mentioned, we refrain from attempting a direct transformation of 1-σ errors and present our results in their respective prior spaces as-is.

Another point of caution pertains to the case of fiducial models closer to GR, such as F6, for which the lower limit of the constraint can approach zero (as is the case with our result plots, Figs. 3 and 6). Our way of representing the results with both the upper and lower limits in the log prior, as well as the choice of the log prior itself in this case, are intended primarily to align with previous works in the literature as aforesaid (e.g., see Fig. 10 of [83]), in order to allow direct comparison with them. We note, however, that considering the attainable precision of experiments in the near future, it can be challenging to observationally distinguish the lower limit from zero, in which case the upper limit carries more observational value.

Under the Gaussian likelihood distribution assumption described previously, we employ the Fisher formalism [103,104],

$$F_{ij} = \sum_{\alpha\beta} \frac{\partial f_\alpha}{\partial p_i} \mathrm{Cov}^{-1}[f_\alpha, f_\beta] \frac{\partial f_\beta}{\partial p_j}, \tag{23}$$

where $f_{\alpha,\beta}$ are the observables in bins labeled by α, β; Cov is the observable covariance matrix and p_i and p_j are a pair of the model parameters being constrained.

The constraints by cluster abundances, as discussed in II B, are represented by $\sigma_8(z)$. In particular, the observables f_α are the set of $\{\sigma_{8(\mathrm{MG})}(z)/\sigma_{8(\Lambda\mathrm{CDM})}(z)\}$ across 30 linearly spaced redshift bins centered on $z = 0.05$ to $z = 2.95$, which are predicted by the MG models. The observable covariance matrix $\mathrm{Cov}^{-1}[f_\alpha, f_\beta]$ on $\sigma_8/\sigma_{8(\Lambda\mathrm{CDM})}$, obtained from [40], is diagonal and is a model-independent result where the errors from the background ΛCDM parameters are marginalized over, reducing the parameters to constrain in (23) to the pair $\{f_{R0}, n\}$ ($f(R)$) or n_{nDGP} (nDGP). Hence, the partial derivative stepsizes for the background cosmology parameters are aligned with that specified in [40]. For the near-GR case, we take a stepsize of 10^{-8} directly with respect to f_{R0}, addressing a linear deviation from GR, with also noting that $\log_{10}(f_{R0})$ is not well-defined. For F5 and F6, the partial derivatives are taken with respect to $\{\log_{10}(f_{R0}), n\}$, with the respective stepsizes $\{0.05, 0.05\}$. In N1 and N5, the stepsize is 0.05 for n_{nDGP}. A five-point central differences scheme is applied to evaluating the partial derivatives over all the MG parameters, giving a third-order accuracy, with the exception of the near-GR case where only a one-sided derivative is feasible due to the $f_{R0} \geq 0$ limitation. For this, a corresponding four-point forward differences scheme is then applied to maintain the third-order accuracy. The priors of the parameters for cluster abundances are inherited from [40], where information from the CMB is included and the priors are discussed and marginalized over (see around Table II of [40]).

For galaxy clustering the observables are the galaxy correlation function multipoles, $f_\alpha = \{\xi_0(s), \xi_2(s), \xi_4(s)\}$, considered over 35 spatial separation bins equally (logarithmically) spaced in the range $25 < s < 600\,(\mathrm{Mpc}/h)$. The cosmological parameters, p_i, are those given in Table I, while the covariance matrix for the monopole, quadrupole and hexadecapole moments is described in the Appendix. Our evaluation assumes a DESI-like survey with LRG and ELG galaxy samples in the redshift range $0.15 < z < 1.85$, using 18 linearly spaced z bins, as outlined in [91]. Our choices for the galaxy number density, survey volume and linear bias as a function of redshift are informed by [91], in particular its Table V. This assumes a mean galaxy number density of $\bar{n}_g \sim 2.5 \times 10^{-4}\,(\mathrm{Mpc}/h)^{-3}$ and $\bar{n}_g \sim 5 \times 10^{-4}\,(\mathrm{Mpc}/h)^{-3}$, for LRGs and ELGs, respectively. The partial derivatives of the multipoles are evaluated with a two-point central differences scheme, with the derivative step-sizes with respect to the background ΛCDM parameters and linear bias provided by [40]. With regards to the MG parameters, in the near-GR case with $f_{R0} \to 0$, we again employ a three-point forward differences scheme, with a forward step of 10^{-8} in f_{R0} while keeping n fixed; the derivative steps for the $\{f_{R0}, n\}$ pair in the F5 and F6 cases are $\{2 \times 10^{-6}, 0.4\}$ and $\{3 \times 10^{-7}, 0.4\}$, respectively, and for n_{nDGP} in the N1 and N5 models they are 0.15 and

0.5. The step-size when differentiating with respect to the nuisance parameter α_σ is 1.5, informed by the detailed study in [53]. We have checked that all of the choices above provide numerical stability in the derivatives. For galaxy clustering, no prior information was added for any of the parameters. The exploration of how to optimally include the BAO information, for example, would require additional appropriate priors (e.g., from big bang nucleosynthesis) on the baryon density parameter $\Omega_b h^2$, a task we reserve for future study.

III. RESULTS

In this section we present the forecasted constraints on the cosmological parameters of Table I from galaxy clustering, and constraints on the MG parameters using combined observables, following the methods outlined previously.

In Fig. 2, we present two-dimensional constraints from each parameter pair in the Fisher analysis, as obtained by the first three nonvanishing multipoles of the redshift-space correlation function of the LRG and ELG galaxy samples, both when considered separately and combined. In addition to the constraints on the standard ΛCDM parameters in line with previous works in the literature (e.g., [91]), the complementarity of the LRG- and the ELG-derived contributions allows us to tightly constrain the pair of the MG parameters $\{\log_{10}(f_{R0}), n\}$, which are the focus of our analysis. We see from the plot that the combined constraints from the two samples on the MG parameters are much tighter than the individual ones. It is also expected that

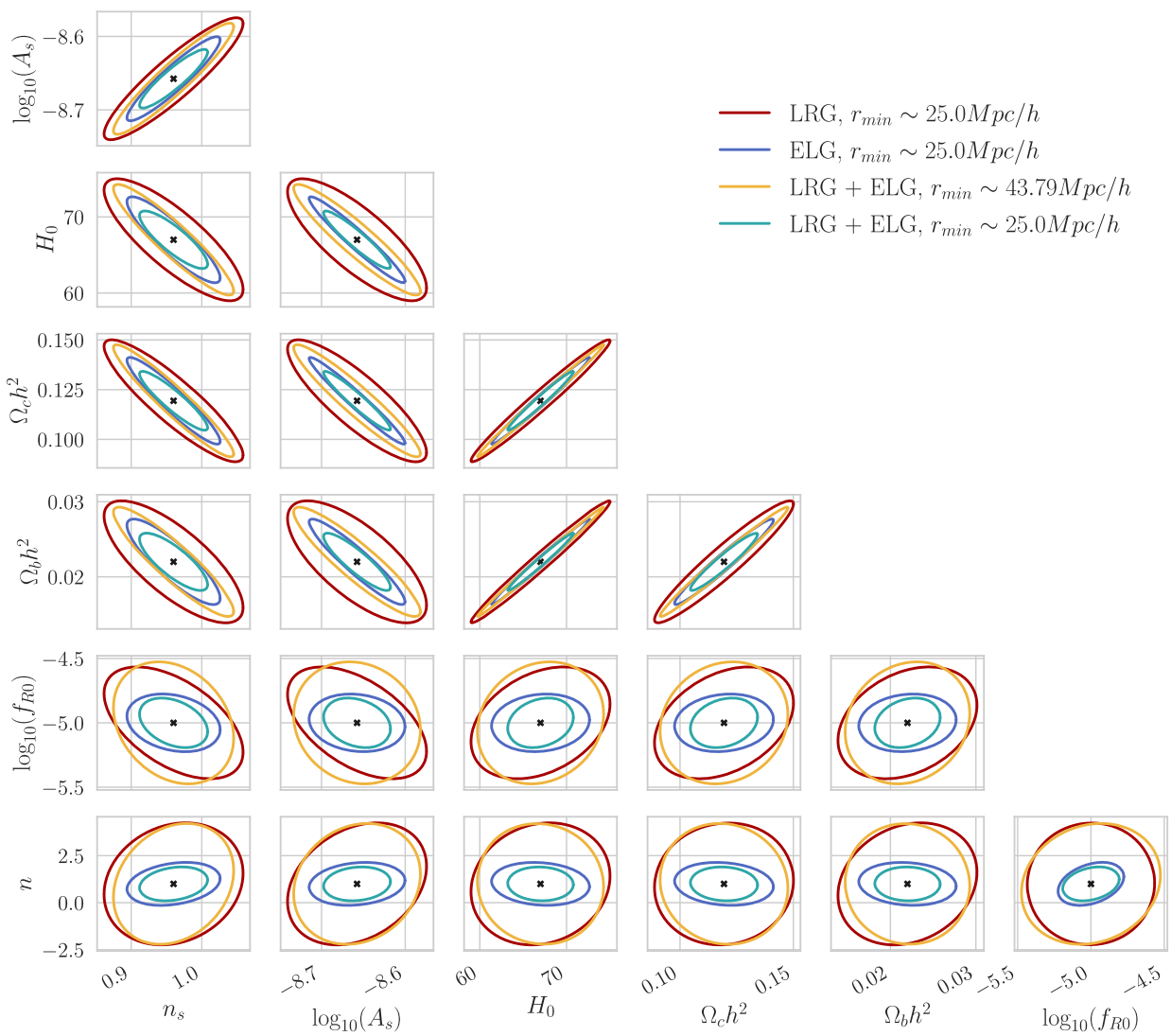

FIG. 2. Galaxy clustering constraints on the parameters in the F5 case (fiducial values $f_{R0} = 10^{-5}$, $n = 1$) using the DESI LRG sample [red], the ELG sample [blue] and both combined [cyan] for a minimum survey scale of $r_{\min} \sim 25.0$ Mpc$/h$, the smallest scale we anticipate can be probed with the survey. Combined constraints for a more conservative minimum scale of $r_{\min} \sim 43.79$ Mpc$/h$ [yellow] are also presented to show the impact of scale on the constraints.

TABLE II. Marginalized one-parameter errors in MG models, presented using galaxy clustering (minimum survey scale $r_{\rm min} \sim 25.0$ Mpc$/h$) and cluster abundances alone respectively, and cross-combining the two observables. The numerical values within the same row of a fiducial parameter denotes the 1-σ (68% confidence) errors on the same parameter around that fiducial value. Specifically for the near-GR case (the top-row for the $f_{R0} = 0$ fiducial value), the 2-σ (95% confidence) upper limits are reported.

	Model	Fiducial parameters	Galaxy clustering: LRG	Galaxy clustering: ELG	Galaxy clustering: ELG + LRG	Cluster abundances	Combined
2-σ	$f(R)$ near-GR	$f_{R0} = 0$	$\leq 1.79 \times 10^{-6}$	$\leq 1.15 \times 10^{-6}$	$\leq 8.64 \times 10^{-7}$	$\leq 7.53 \times 10^{-7}$	$\leq 5.68 \times 10^{-7}$
1-σ	$f(R)$ F5	$\log_{10}(f_{R0}) = -5$	0.29	0.15	0.13	0.37	0.12
		$n = 1$	2.14	0.75	0.59	1.00	0.36
	$f(R)$ F6	$\log_{10}(f_{R0}) = -6$	1.78	1.12	0.77	0.69	0.48
		$n = 1$	8.64	5.92	3.61	3.31	2.30
	nDGP N1	$n_{\rm nDGP} = 1$	0.59	0.25	0.23	0.094	0.087
	nDGP N5	$n_{\rm nDGP} = 5$	8.30	3.63	3.29	1.77	1.56

using the ELGs produces tighter constraints in all parameter planes, given that this sample has a larger number density and redshift range, compared to the LRG counterpart (see Table V of [91]).

Figure 2 also shows, as we further quantify in Table II, that the forecasted constraints on the MG parameter $\log_{10}(f_{R0})$ are at least about an order of magnitude tighter compared to the parameter n. This finding is attributed to the fact that the two-point function is more sensitive to variations of f_{R0} than of n, in particular for the range of scales we consider in this work, as was found by the sensitivity analysis of [102]. Due to this fact, most previous works in the literature (e.g., [83,105]) have commonly worked with a fixed value of $n = 1$, and only considered constraints on f_{R0}. Thanks to our flexible analytical model for the anisotropic correlation function in any scalar-tensor theory, in this work we are able to provide constraints on the fuller parameter space of the $f(R)$ Hu-Sawicki model.

In addition, in Fig. 2 we demonstrate how the choice of the minimum survey scale impacts the constraints we obtain, finding that a more conservative value of $r_{\rm min} \sim 43.79$ Mpc$/h$ dilutes the constraining power overall. We find that the constraints from LRG + ELG combined for this more conservative value are comparable with the constraints from LRGs alone for $r_{\rm min} \sim 25.0$ Mpc$/h$. This reduction in sensitivity is consistent with the predicted deviations in the Hu-Sawicki model becoming progressively more pronounced, as one considers smaller scales. As a result, an analysis focusing on larger scales would restrict the ability to probe MG signals, resulting in looser constraints on the corresponding MG parameters.

For the F6 model, we find that the 2D degeneracies between the ΛCDM and MG parameters are qualitatively similar to those for F5. In Fig. 3 we show that the constraints on the two MG parameters are comparatively looser in F6 versus F5, consistent with the predicted deviations from GR being smaller. We find that the F6 constraints from LRG and ELG data are more comparable, with ELGs still being tighter, so that the combination of the two gives more notable relative improvements to the ELG data alone than for the F5 scenario. As we have discussed in Sec. II D, for the F6 case the upper limit is more effectively represented under considerations of future experiments,

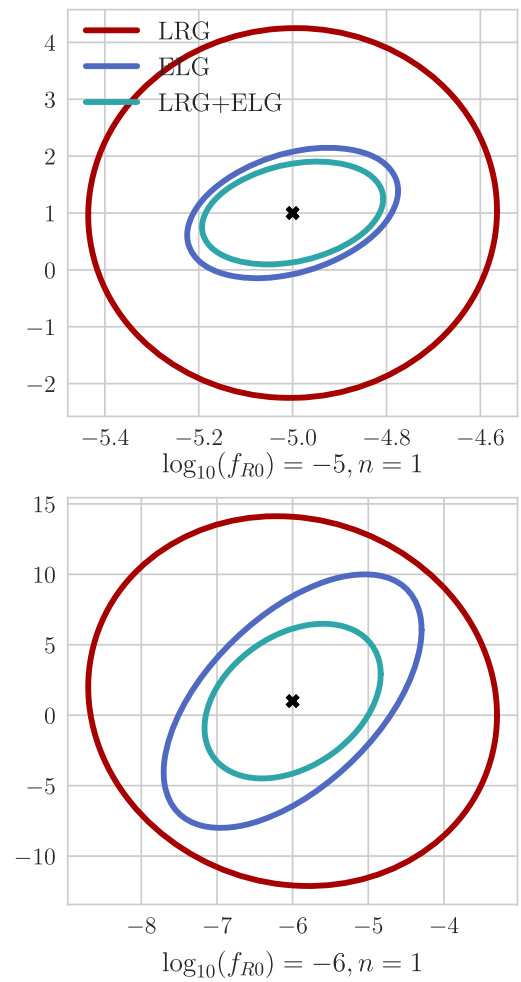

FIG. 3. Galaxy clustering constraints on $\{\log_{10}(f_{R0}), n\}$ in the F5 (top) and F6 (bottom) cases (fiducial values $f_{R0} = 10^{-5}$ and 10^{-6}, $n = 1$) for the LRG sample [red], ELG sample [blue] and both combined [cyan] assuming $r_{\rm min} \sim 25.0$ Mpc$/h$.

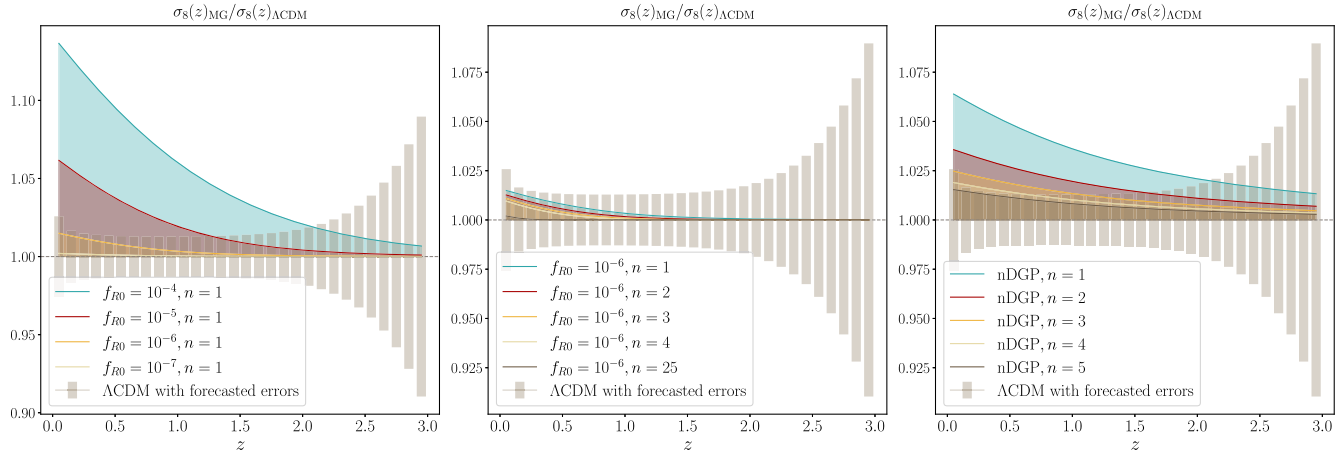

(a) Varying f_{R0}, $n = 1$ (b) Varying n, $f_{R0} = 10^{-6}$ (c) Varying n, for nDGP

FIG. 4. The MG predicted $\sigma_8(z)_{\rm MG}/\sigma_8(z)_{\Lambda\rm CDM}$ normalized at $z = 10$, plotted against the error of this ratio forecasted by cluster abundances. Left, (a): shows scenarios with different f_{R0} values while fixing n in $f(R)$ as 1. Center, (b): shows scenarios fixing $f_{R0} = 10^{-6}$ while changing n. Right, (c): shows the case in nDGP, where $n_{\rm nDGP}$ is varied.

and while we use the log space to ease comparison with the literature, we caution against the translation of the constraints to the linear space.

We also performed the same analysis on the nDGP models but will only present the final combined constraints and omit showing the full corner plots for the sake of brevity. Our findings regarding nDGP are overall similar to the $f(R)$ scenario: the direction of the degeneracies for the background ΛCDM parameters are the same, while the degeneracies are stronger for the nDGP scenarios, presumably due to the scale-independence.

The 1D projected uncertainties obtained from galaxy clustering for the near-GR, F5, F6 $f(R)$ model and nDGP are summarized in Table II. Across all the models considered, the uncertainties are principally driven by the ELG galaxy sample. For the near-GR case, the combination of LRGs with ELGs tightens the constraint on f_{R0} from ELGs alone by 25% (with the ELG constraint being about two-thirds that from LRGs). For F5, the ELG constraints on both parameters are roughly half the size of those from LRGs, and the combination of the two only reduces the uncertainties by 10%–20%. The impact of combining the two is more pronounced for F6, with ELG + LRG constraints about 30%–40% tighter than for ELGs alone. For both nDGP cases, the ELG constraint error on the $n_{\rm nDGP}$ parameter is less than half of that from LRGs alone, and only a ∼10% reduction is obtained by combining the two samples.

Our constraints for the $f(R)$ and nDGP cases are of the same order as the ones presented in [105], which performed a Markov chain Monte Carlo analysis.

We now consider the constraints from cluster abundances, obtained from $\sigma_{8(\rm MG)}/\sigma_{8(\Lambda\rm CDM)}$. In Fig. 4, we provide an overview comparison of the evolution of the predicted σ_8 ratio, over the 30 redshift bins from $z = 0.05$ to $z = 2.95$, for the MG models versus the model-independent forecasted errors for future observations at the Simons Observatory [31]. The ratios predicted from MG are normalized at $z = 10$, consistent with the assumption that MG gives indistinguishable predictions from ΛCDM for LSS at high redshifts, varying $\{f_{R0}, n\}$ for $f(R)$ and n for nDGP, respectively. The $\sigma_{8(\Lambda\rm CDM)}$ is normalized to be that calculated from (7) (with $g_{\rm eff} = 0$).

This overview provides an insight into the sensitivity of σ_8 with respect to the parameters of the two MG models we consider. For both the $f(R)$ and nDGP MG models, the constraining power mainly lies at lower redshifts, at $z < 2$, increasing as one approaches $z = 0$, where the deviation of the MG-predicted σ_8 is the highest, and the forecasted errors by cluster abundances are the tightest, notably for $0.5 < z < 1.5$. Furthermore, by comparing the signal to errors for the $f(R)$ case in subfigures (a) and (b), we anticipate that the σ_8 data will be more sensitive to variations in f_{R0} than in n.

As is the case for galaxy clustering, we also summarize the model parameter constraints from galaxy cluster abundances in Table II. We find that for the near-GR case in $f(R)$, the constraints from cluster abundances and that from galaxy clustering are comparable. However, when it comes to constraining the model that deviates most greatly from GR, with a fiducial $\log_{10}(f_{R0}) = -5$, cluster abundances are not found to be as competitive as galaxy clustering. For this model, the constraint on $\log_{10}(f_{R0})$ is a factor of 2.8 larger, while for n it is 70% larger. Cluster abundances then provide comparatively tighter constraints as we move to the weaker $f(R)$ model, with fiducial $\log_{10}(f_{R0}) = -6$, where the constraints on $\log_{10}(f_{R0})$ and n, although effectively more of an upper limit, are roughly 10% smaller than those predicted from galaxy clustering. We also find that cluster abundances provide constraints on the nDGP parameters

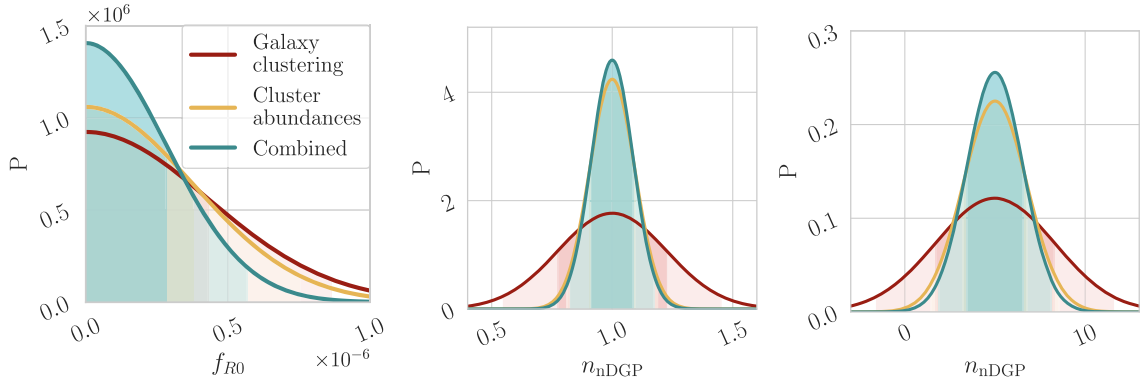

(a) f_R: near-GR (fiducial $f_{R0} = 0$) (b) nDGP: fiducial $n_{\rm nDGP} = 1$ (c) nDGP: fiducial $n_{\rm nDGP} = 5$

FIG. 5. The 1D likelihood distribution for [Left, (a)] the near-GR $f(R)$ model, with fiducial value $f_{R0} = 0$ (the value of n becomes redundant) and for the nDGP model with fiducial values [Center, (b)] $n_{\rm nDGP} = 1$ and [Right, (c)] $n_{\rm nDGP} = 5$, under a Gaussian assumption in the Fisher forecast. The constraints from [red] galaxy clustering (ELG + LRG), [yellow] cluster abundances and [cyan] the two combined are shown, with the darker fill-in shades denoting the corresponding 1-σ (68%) confidence levels, lighter shades the 2-σ (95%) confidence levels.

that are roughly 50%–60% tighter than those from galaxy clustering.

We now present our findings in figures. We first examine the near-GR $f(R)$ case in Fig. 5(a), which is conveniently placed alongside the corresponding nDGP constraints, due to that they are all one-dimensional. As we mentioned, the relative impacts of the cluster abundance and galaxy clustering constraints on f_{R0} are comparable for each dataset, and the combination provides a ~25% improvement in the 1-σ constraint relative to that from cluster abundances alone. This result also implies that a 2-σ (95% confidence) upper limit of $f_{R0} \leq 5.68 \times 10^{-7}$ can be placed for f_{R0} when we take the fiducial scenario as GR ($f_{R0} = 0$).

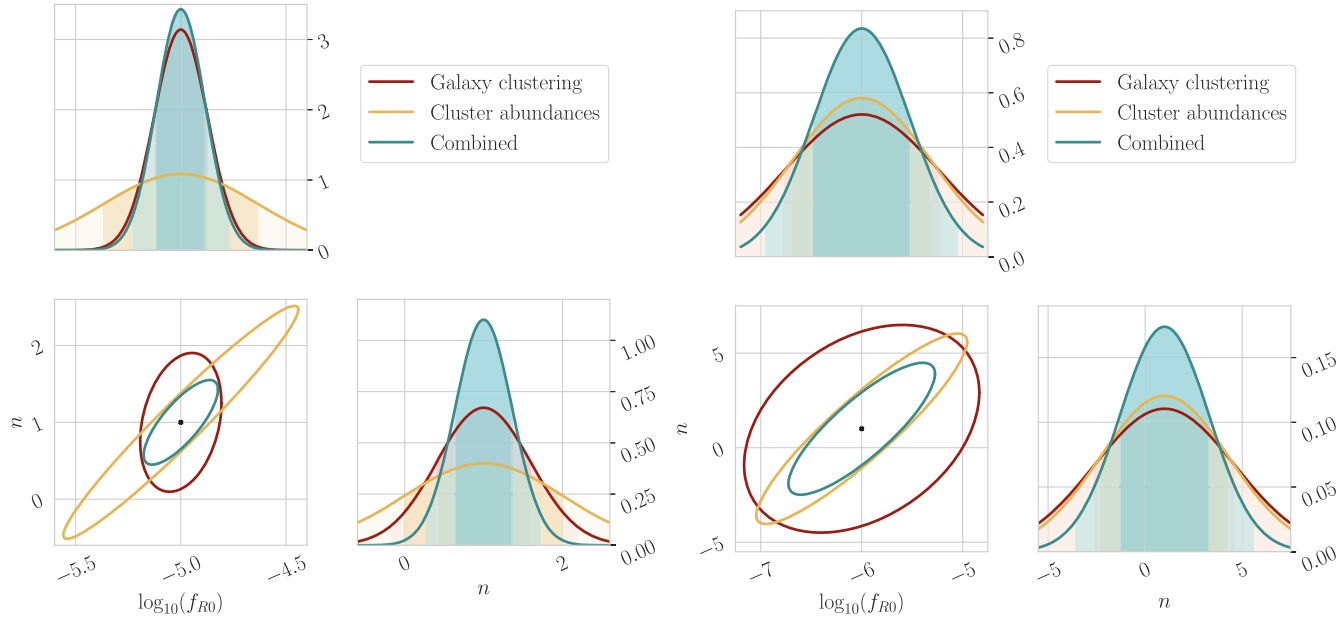

(a) $f(R)$: F5 (fiducial $\log_{10}(f_{R0}) = -5$) (b) $f(R)$: F6 (fiducial $\log_{10}(f_{R0}) = -6$)

FIG. 6. The constraints on the [(a)] F5 and [(b)] F6 $f(R)$ scenarios are shown from [red] galaxy clustering, [yellow] cluster abundances and [cyan] the two combined. The covariance ellipses in the $\{\log_{10}(f_{R0}), n\}$ parameter space indicating the joint 1-σ (68%) confidence levels, and their respective marginalized 1D Gaussian likelihoods are shown for each scenario, with the darker fill-in shades denoting the corresponding 1-σ (68%) confidence levels, lighter shades the 2-σ (95%) confidence levels.

We then present the 2D $\{\log_{10}(f_{R0}), n\}$ constraints for the F5 and F6 $f(R)$ scenarios for the two datasets in Fig. 6, with the corresponding combined 1D constraints summarized in Table II. The choice of our prior space and the corresponding caveats have been discussed in Sec. II D and also noted in the captions. For F5 with cluster abundances we find that there is a strong degeneracy in the $\log_{10}(f_{R0})$-n plane but with a well-measured combination in the direction orthogonal to the degeneracy. This phenomenon has been tested to be relatively stable across the higher and lower redshift ranges. In contrast, constraints from galaxy clustering do not show significant degeneracies in this parameter space and provide tighter constraints on $\log_{10}(f_{R0})$ and n separately, but with an overall likelihood ellipse that is wider (the best constraint in the 2D plane is weaker than for the cluster abundances). In combination, the galaxy clustering constraints help break the degeneracy from the cluster abundance data and drive the constraints on $\log_{10}(f_{R0})$. The constraints on n are improved, relative to those from the galaxy clustering, by a factor of $\sim$2. For F6, the constraints from both cluster abundances and galaxy clustering are weaker, but the galaxy clustering constraints on $\log_{10}(f_{R0})$ are comparable to those from the cluster abundances. The net effect of combining the two datasets is less significant than for F5; however, we see improvements of $\sim$30% in constraints on both $\log_{10}(f_{R0})$ and n.

The constraints on the nDGP model parameter are also shown in Fig. 5. Here we find that the cluster abundances drive the constraints for both fiducial scenarios and the galaxy clustering plays a minimal role in affecting improvements, which possibly is also due to the scale-independence that nDGP features.

Spanning the two most popular classes of screening in the literature, through the representative $f(R)$ and nDGP MG models, our detailed analysis overall serves to highlight the ways in which the upcoming precise observations of redshift-space galaxy clustering and cluster abundances will enable us to probe the landscape of dark energy and MG parametrizations in the next 10 years. The nDGP model realizes the Vainshtein screening mechanism, which is harder to constrain using other astrophysical probes, in comparison to the chameleon screening of $f(R)$. Here we find that the cluster abundances are better able to constrain the scale-independent effects of the nDGP model, while the galaxy clustering provides tighter constraints on the scale-dependent $f(R)$ scenario, and could break degeneracies when combined with cluster abundances. This complementarity of the two techniques in constraining these models, and the potential for cluster abundances to constrain nDGP, are important outcomes from our findings.

IV. DISCUSSION

In this work we performed a detailed study of our ability to constrain the large-scale properties of gravity with a combination of two promising probes of the LSS: galaxy clustering from spectroscopic observations by DESI as well as cluster abundances from tSZ observations by the Simons Observatory.

For galaxy clustering, we employ the Gaussian streaming model with Lagrangian perturbation theory (LPT) to predict the anisotropic redshift-space two-point correlation function of biased tracers, which was recently generalized to support predictions for MG parametrizations. We apply the model to predict the multipoles of the RSD correlation function for the ELG and the LRG DESI spectroscopic galaxy samples as well as their corresponding covariance matrices. Regarding cluster abundances, we use the amplitude of density fluctuations, $\sigma_8(z)$, obtained by tSZ-selected galaxy clusters, as a window into the nature of the underlying gravity model, expanding upon recent detailed model-independent studies in the context of standard cosmological parameters.

We employ the Fisher forecast formalism to obtain a set of joint constraints on two widely studied MG models, the Hu-Sawicki $f(R)$ and the nDGP gravity models. We demonstrate that the two independent probes complement each other in constraining the Hu-Sawicki $f(R)$ model parameters, for a near-GR fiducial scenario, as well as varying degrees of deviation away from a ΛCDM background. We find that the tightest constraints are obtained in the large-deviation F5 scenario, at the level of a $\sim$2% forecasted joint constraint on the $\log_{10}(f_{R0})$ parameter, with the ELGs serving as the primary source of discriminating power on the galaxy clustering side. The constraining power of both probes is primarily derived from their corresponding lower redshift snapshots, when the MG deviations are more pronounced overall. We also consider the full 2D parameter space, $\{\log_{10}(f_{R0}), n\}$, for the Hu-Sawicki model, and place corresponding constraints.

In a similar manner, we find that the interplay between the cluster abundance and galaxy clustering observables can be utilized to constrain the parameter space of the nDGP gravity scenario. We forecast a combined relative constraint of $\sim$9% in the $n_{\rm nDGP} = 1$ case and that the cluster abundance observations would principally drive these constraints. This, and the opposite phenomenon that galaxy clustering drives the constraints for the F5 scenario, are potentially due to the fact that the $f(R)$ model is scale-dependent in contrast to nDGP in linear and quasilinear scales, which might also explain the relatively balanced constraining powers of the two observables for F6 and near-GR, where the scale-dependence is weaker than in F5.

There are many possible ways in which one can expand upon this line of inquiry. For galaxy clustering, the accuracy of our model can be further improved by including the one-loop corrections of LPT [53] into the GSM prediction, as well as by introducing effective field theory corrections to account for nonperturbative small-scale physics. Such an approach would also need to be combined

with a suitably improved treatment of the clustering covariance matrix, which we assumed to be Gaussian in the present work. Furthermore, it would be very interesting to also explore the constraining power of the Fourier space counterpart of the two-point function, the redshift space power spectrum, obtained either by analytical approaches (see e.g., [97]) or through emulators [102]. For galaxy cluster abundances, extending this work to a full Fisher analysis with MG requires halo mass functions [e.g., 106] with fitting formulas in their *ansatz* for the Hu-Sawicki $f(R)$ and the nDGP gravity models. We expect these constraints to further improve with CMB-S4 cluster abundances in combination with photometric and weak gravitational lensing observations by stage-IV surveys such as the V. Rubin Observatory LSST [47,48]. Finally, it would be interesting to use a Markov chain Monte Carlo forecasting approach to see how non-Gaussianities in the posterior likelihood impact the constraints and degeneracies we present.

In the near future, synergies between new cosmological surveys will allow us to explore the vast landscape of dark energy and MG scenarios, and shed new light on the nature of cosmic acceleration. Our work serves to highlight the great promise held in such considerations, as well as the optimal ways in which the vast amounts of upcoming observations could be utilized.

ACKNOWLEDGMENTS

The authors would like to thank Mathew Madhavacheril for helpful discussions regarding the cluster abundances analysis as well as code resources that helped plotting the covariance ellipses. G. V. would like to thank Sukhdeep Singh and Yin Li for useful discussions on analytical models of covariance matrices. This work is not an official Simons Observatory paper. G. V.'s work is supported by NSF Grant No. AST-1813694. G. V. and R. B. acknowledge support from DOE Grant No. DE-SC0011838, NASA ATP Grant No. 80NSSC18K0695, NASA ROSES Grant No. 12-EUCLID12-0004 and funding related to the Roman High Latitude Survey Science Investigation Team. N. B. acknowledges support from NSF Grant No. AST-1910021.

APPENDIX: COVARIANCE MATRIX CALCULATION

This Appendix provides the details of the analytical model we use to evaluate the covariance matrix of the multipoles of the anisotropic correlation function. We begin with the known expression for the Poisson error matrix of the power spectrum, assuming Gaussian density perturbations [107,108]:

$$\mathrm{Cov}[P(\mathbf{k}),P(\mathbf{k}')] = \frac{(2\pi)^3}{V_s}\left(P\left(\mathbf{k}+\frac{1}{n}\right)^2(\delta_D(\mathbf{k}-\mathbf{k}')+\delta_D(\mathbf{k}+\mathbf{k}'))\right) + \frac{1}{n^2V_s}[P(|\mathbf{k}-\mathbf{k}'|)+P(|\mathbf{k}+\mathbf{k}'|)+2P(\mathbf{k})+2P(\mathbf{k}')]+\frac{1}{n^3V_s}, \tag{A1}$$

with n the number density of the galaxies in a given sample, V_s the survey of the volume and δ_D the Dirac delta-function. The second and third lines on the r.h.s of Eq. (A1) encode the Poisson shot noise contributions to the covariance matrix [109]. Equation (A1) has neglected contributions from nonlinear gravitational evolution [108,110–112], super sample covariance [113–117] and effects of the survey nontrivial window function [118].

Our goal is to Fourier transform the result (A1), so that we obtain the configuration space equivalent expression for the covariance matrix of the anisotropic correlation function. In the simpler case of real space considerations, with the correlation function being isotropic, [109] demonstrated that, by angle-averaging the Fourier transform of (A1), the oscillatory Bessel function dependencies can be eliminated (unlike in the RSD case, as shown below), and a more compact expression is possible. [109] also found the Poisson shot-noise contributions to be diagonal for the correlation function. In redshift space, which is what we are interested in this work, the equivalent configuration space expression for (A1) has been derived in [119,120], assuming only Gaussian shot-noise contributions (i.e., neglecting the second and third lines in the r.h.s of (A1), and is the following:

$$\mathrm{Cov}[\xi_{l_1}(s_i),\xi_{l_2}(s_j)] = \frac{i^{l_1+l_2}}{2\pi^2}\int_0^\infty k^2\sigma^2_{l_1l_2}(k)j_{l_1}(ks_i)j_{l_2}(ks_j)dk, \tag{A2}$$

where we defined the multipole per-mode covariance:

$$\sigma^2_{l_1l_2}(k) = \frac{(2l_1+1)(2l_2+1)}{V_s} \times \int_{-1}^{1}\left[P(k,\mu_k)+\frac{1}{n}\right]^2 L_{l_1}(\mu_k)L_{l_2}(\mu_k)d\mu_k, \tag{A3}$$

where $j_{l_1}(ks_i)$, $j_{l_2}(ks_j)$ are the spherical Bessel functions of the first kind. Poisson shot-noise contributions can potentially become significant, as pointed out by [109]. To that end, we proceed to expand the expression (A2) to also

include the Poisson terms to the shot-noise contributions, just as in the real-space version of [109]. To do so, we first adopt our convention for the Fourier transformation, applied on the correlation function:

$$\xi(\mathbf{s}) = \int \frac{d^3k}{(2\pi)^3} e^{i\mathbf{k}\cdot\mathbf{s}} P(\mathbf{k}), \tag{A4}$$

and label the terms reflecting the Poisson shot-noise contributions in (A1) (second and third lines of r.h.s) as $\mathrm{Cov}[P(\mathbf{k}), P(\mathbf{k}')]|_{\mathrm{Poisson}}$. Fourier transforming both sides then gives[2]

$$\mathrm{Cov}[\xi(\mathbf{s}_i), \xi(\mathbf{s}_j)]|_{\mathrm{Poisson}} = \frac{2}{n^2 V_s} \xi(\mathbf{s}_i) \delta_D(\mathbf{s}_i - \mathbf{s}_j). \tag{A5}$$

Finally, we aim to project out the correlation function multipoles, for which we integrate the ξ terms on the l.h.s above (after multiplying both sides with the appropriate Legendre polynomials), as in (22), which gives

$$\begin{aligned}&\mathrm{Cov}[\xi_{l_1}(s_i), \xi_{l_2}(s_j)]|_{\mathrm{Poisson}} \\ &= \frac{(2l_1+1)(2l_2+1)}{n^2 V_s 4\pi s_i^2} \delta_D(s_i - s_j) \\ &\quad \times \int_{-1}^{1} \xi(s_i, \mu_s) L_{l_1}(\mu_s) L_{l_2}(\mu_s) d\mu_s,\end{aligned} \tag{A6}$$

where we have made use of the delta-function property:

$$\delta_D(\mathbf{s}_i - \mathbf{s}_j) = \frac{\delta_D(s_i - s_j)}{s_i^2} \delta_D(\Omega_i - \Omega_j), \tag{A7}$$

with Ω denoting the corresponding solid angles. Combining (A6) with (A2), we arrive at the desired result:

$$\begin{aligned}&\mathrm{Cov}[\xi_{l_1}(s_i), \xi_{l_2}(s_j)] \\ &= \frac{i^{l_1+l_2}}{2\pi^2} \int_0^\infty k^2 \sigma_{l_1 l_2}^2(k) j_{l_1}(ks_i) j_{l_2}(ks_j) dk \\ &\quad + \frac{(2l_1+1)(2l_2+1)}{n^2 V_s 4\pi s_i^2} \delta_D(s_i - s_j) \\ &\quad \times \int_{-1}^{1} \xi(s_i, \mu_s) L_{l_1}(\mu_s) L_{l_2}(\mu_s) d\mu_s,\end{aligned} \tag{A8}$$

which is the equation we use to evaluate the covariance matrix of the multipoles of ξ in this work. The last term in Eq. (A8) expands the Gaussian expression (A2) of [119,120] in order to also capture the Poisson shot-noise contributions in the anisotropic case, and exhibits the same diagonal nature as the corresponding real space expression of Eq. (32) in [109], which it recovers in the limit of isotropy. The shot-noise terms in (A8) are further divided by the bin width, Δs, in order to avoid overestimating the error predictions, as in [109,121].

To summarize our procedure, after getting an analytical prediction for the RSD correlation function for our desired cosmology from Eq. (17), we use it to predict the covariance matrix from Eq. (A8) (combined with the input from (A3)). An intermediate step is to Fourier Transform to also obtain $P(k, \mu_k)$ from $\xi(s, \mu_s)$, which is required in Eq. (A3), and can be easily performed with the publicly available package `mcfit`.[3] The integrals involving spherical Bessel functions in (A2) can also be conveniently performed by utilizing the same package.

[2]The Fourier transformation of the r.h.s gives rise to additional terms involving delta-functions, as in [109], that only contribute at separations $r = 0$, and are thus dropped.

[3]https://github.com/eelregit/mcfit

[1] S. Perlmutter *et al.* (Supernova Cosmology Project), Measurements of omega and lambda from 42 high-redshift supernovae, Astrophys. J. **517**, 565 (1999).

[2] A. G. Riess *et al.* (Supernova Search Team), Type Ia supernova discoveries at $z > 1$ from the hubble space telescope: Evidence for past deceleration and constraints on dark energy evolution, Astrophys. J. **607**, 665 (2004).

[3] D. J. Eisenstein *et al.* (SDSS Collaboration), Detection of the baryon acoustic peak in the large-scale correlation function of SDSS luminous red galaxies, Astrophys. J. **633**, 560 (2005).

[4] W. J. Percival, S. Cole, D. J. Eisenstein, R. C. Nichol, J. A. Peacock, A. C. Pope, and A. S. Szalay, Measuring the baryon acoustic oscillation scale using the SDSS and 2dFGRS, Mon. Not. R. Astron. Soc. **381**, 1053 (2007).

[5] W. J. Percival, B. A. Reid, D. J. Eisenstein, N. A. Bahcall, T. Budavari, J. A. Frieman, M. Fukugita, J. E. Gunn, Ž. Ivezić, G. R. Knapp *et al.*, Baryon acoustic oscillations in the sloan digital sky survey data release 7 galaxy sample, Mon. Not. R. Astron. Soc. **401**, 2148 (2010).

[6] E. A. Kazin, J. Koda, C. Blake, N. Padmanabhan, S. Brough, M. Colless, C. Contreras, W. Couch, S. Croom,

D. J. Croton *et al.*, The WiggleZ dark energy survey: Improved distance measurements to $z = 1$ with reconstruction of the baryonic acoustic feature, Mon. Not. R. Astron. Soc. **441**, 3524 (2014).

[7] D. Spergel, N. Gehrels, J. Breckinridge, M. Donahue, A. Dressler *et al.*, Wide-field infrared survey telescope-astrophysics focused telescope assets WFIRST-AFTA final report, arXiv:1305.5422.

[8] P. A. R. Ade, N. Aghanim, C. Armitage-Caplan, M. Arnaud, M. Ashdown, F. Atrio-Barandela, J. Aumont, C. Baccigalupi, A. J. Banday *et al.* (Planck Collaboration), Planck 2013 results. XVI. Cosmological parameters, Astron. Astrophys. **571**, A16 (2014).

[9] P. A. R. Ade *et al.* (Planck Collaboration), Planck 2015 results. XIII. Cosmological parameters, Astron. Astrophys. **594**, A13 (2016).

[10] C. Wetterich, Cosmology and the fate of dilatation symmetry, Nucl. Phys. **B302**, 668 (1988).

[11] B. Ratra and P. J. E. Peebles, Cosmological consequences of a rolling homogeneous scalar field, Phys. Rev. D **37**, 3406 (1988).

[12] E. J. Copeland, M. Sami, and S. Tsujikawa, Dynamics of dark energy, Int. J. Mod. Phys. D **15**, 1753 (2006).

[13] S. Weinberg, The cosmological constant problem, Rev. Mod. Phys. **61**, 1 (1989).

[14] K. Koyama, Cosmological tests of modified gravity, Rep. Prog. Phys. **79**, 046902 (2016).

[15] M. Ishak, Testing general relativity in cosmology, Living Rev. Relativity **22**, 1 (2019).

[16] P. G. Ferreira, Cosmological tests of gravity, Annu. Rev. Astron. Astrophys. **57**, 335 (2019).

[17] C. M. Will, The confrontation between general relativity and experiment, Living Rev. Relativity **9**, 3 (2006).

[18] B. Abbott, R. Abbott, T. Abbott, F. Acernese, K. Ackley, C. Adams, T. Adams, P. Addesso, R. Adhikari, V. Adya *et al.*, GW170817: Observation of Gravitational Waves from a Binary Neutron Star Inspiral, Phys. Rev. Lett. **119**, 161101 (2017).

[19] V. Savchenko, C. Ferrigno, E. Kuulkers, A. Bazzano, E. Bozzo, S. Brandt, J. Chenevez, T. J.-L. Courvoisier, R. Diehl, A. Domingo *et al.*, *INTEGRAL* detection of the first prompt gamma-ray signal coincident with the gravitational-wave event GW170817, Astrophys. J. **848**, L15 (2017).

[20] L. Lombriser and A. Taylor, Breaking a dark degeneracy with gravitational waves, J. Cosmol. Astropart. Phys. 03 (2016) 031.

[21] L. Lombriser and N. A. Lima, Challenges to self-acceleration in modified gravity from gravitational waves and large-scale structure, Phys. Lett. B **765**, 382 (2017).

[22] J. Sakstein and B. Jain, Implications of the Neutron Star Merger GW170817 for Cosmological Scalar-Tensor Theories, Phys. Rev. Lett. **119**, 251303 (2017).

[23] J. M. Ezquiaga and M. Zumalacrregui, Dark Energy After GW170817: Dead Ends and the Road Ahead, Phys. Rev. Lett. **119**, 251304 (2017).

[24] P. Creminelli and F. Vernizzi, Dark Energy After GW170817 and GRB170817A, Phys. Rev. Lett. **119**, 251302 (2017).

[25] T. Baker, E. Bellini, P. Ferreira, M. Lagos, J. Noller, and I. Sawicki, Strong Constraints on Cosmological Gravity from GW170817 and GRB 170817A, Phys. Rev. Lett. **119**, 251301 (2017).

[26] W. Hu and I. Sawicki, Models of $f(R)$ cosmic acceleration that evade solar-system tests, Phys. Rev. D **76**, 064004 (2007).

[27] G. Dvali, G. Gabadadze, and M. Porrati, 4D gravity on a brane in 5d minkowski space, Phys. Lett. B **485**, 208 (2000).

[28] D. Huterer, D. Kirkby, R. Bean, A. Connolly, K. Dawson, S. Dodelson, A. Evrard, B. Jain, M. Jarvis, E. Linder *et al.*, Growth of cosmic structure: Probing dark energy beyond expansion, Astropart. Phys. **63**, 23 (2015).

[29] E. V. Linder, Cosmic growth history and expansion history, Phys. Rev. D **72**, 043529 (2005).

[30] M. Ishak *et al.*, Modified gravity and dark energy models beyond $w(z)$CDM testable by LSST, arXiv:1905.09687.

[31] P. Ade, J. Aguirre, Z. Ahmed, S. Aiola, A. Ali, D. Alonso, M. A. Alvarez, K. Arnold, P. Ashton, J. Austermann *et al.* (The Simons Observatory Collaboration), The simons observatory: Science goals and forecasts, J. Cosmol. Astropart. Phys. 02 (2019) 056

[32] M. Levi *et al.* (DESI Collaboration), The DESI experiment, a whitepaper for Snowmass 2013, arXiv:1308.0847.

[33] M. Cataneo, D. Rapetti, F. Schmidt, A. B. Mantz, S. W. Allen, D. E. Applegate, P. L. Kelly, A. von der Linden, and R. G. Morris, New constraints on $f(R)$ gravity from clusters of galaxies, Phys. Rev. D **92**, 044009 (2015).

[34] J.-H. He and B. Li, Accurate method of modeling cluster scaling relations in modified gravity, Phys. Rev. D **93**, 123512 (2016).

[35] B. Li, J.-H. He, and L. Gao, Cluster gas fraction as a test of gravity, Mon. Not. R. Astron. Soc. **456**, 146 (2016).

[36] J. Sakstein, H. Wilcox, D. Bacon, K. Koyama, and R. C. Nichol, Testing gravity using galaxy clusters: new constraints on beyond Horndeski theories, J. Cosmol. Astropart. Phys. 07 (2016) 019.

[37] D. S. Y. Mak, E. Pierpaoli, F. Schmidt, and N. Macellari, Constraints on modified gravity from Sunyaev-Zeldovich cluster surveys, Phys. Rev. D **85**, 123513 (2012).

[38] M. A. Mitchell, J. hua He, C. Arnold, and B. Li, A general framework to test gravity using galaxy clusters I: Modelling the dynamical mass of haloes in $f(R)$ gravity, Mon. Not. R. Astron. Soc. **477**, 1133 (2018).

[39] D. Cromer, N. Battaglia, and M. S. Madhavacheril, Improving constraints on fundamental physics parameters with the clustering of Sunyaev-Zeldovich selected galaxy clusters, Phys. Rev. D **100**, 063529 (2019).

[40] M. S. Madhavacheril, N. Battaglia, and H. Miyatake, Fundamental physics from future weak-lensing calibrated Sunyaev-Zel'dovich galaxy cluster counts, Phys. Rev. D **96**, 103525 (2017).

[41] A. Barreira, B. Li, E. Jennings, J. Merten, L. King, C. Baugh, and S. Pascoli, Galaxy cluster lensing masses in modified lensing potentials, Mon. Not. R. Astron. Soc. **454**, 4085 (2015).

[42] J. E. Bautista, R. Paviot, M. Vargas Magaa, S. de la Torre, S. Fromenteau, H. Gil-Marn, A. J. Ross, E. Burtin,

K. S. Dawson, J. Hou *et al.*, The completed SDSS-IV extended Baryon Oscillation Spectroscopic Survey: Measurement of the BAO and growth rate of structure of the luminous red galaxy sample from the anisotropic correlation function between redshifts 0.6 and 1, Mon. Not. R. Astron. Soc. **500**, 736 (2020).

[43] A. Tamone, A. Raichoor, C. Zhao, A. de Mattia, C. Gorgoni, E. Burtin, V. Ruhlmann-Kleider, A. J. Ross, S. Alam, W. J. Percival *et al.*, The completed SDSS-IV extended Baryon Oscillation Spectroscopic Survey: growth rate of structure measurement from anisotropic clustering analysis in configuration space between redshift 0.6 and 1.1 for the emission-line galaxy sample, Mon. Not. R. Astron. Soc. **499**, 5527 (2020).

[44] A. de Mattia, V. Ruhlmann-Kleider, A. Raichoor, A. J. Ross, A. Tamone, C. Zhao, S. Alam, S. Avila, E. Burtin, J. Bautista *et al.*, The completed SDSS-IV extended baryon oscillation spectroscopic survey: Measurement of the BAO and growth rate of structure of the emission line galaxy sample from the anisotropic power spectrum between redshift 0.6 and 1.1, Mon. Not. R. Astron. Soc. **501**, 5616 (2020).

[45] S. Alam *et al.*, Testing the theory of gravity with DESI: estimators, predictions and simulation requirements, arXiv:2011.05771.

[46] R. Laureijs *et al.* (EUCLID Collaboration), Euclid definition study report, arXiv:1110.3193.

[47] P. A. Abell *et al.* (LSST Science Collaborations, LSST Project), LSST Science Book, Version 2.0, arXiv:0912.0201.

[48] A. Abate *et al.* (LSST Dark Energy Science), Large synoptic survey telescope: Dark energy science collaboration, arXiv:1211.0310.

[49] O. Dor *et al.*, Cosmology with the SPHEREX all-sky spectral survey, arXiv:1412.4872.

[50] N. Kaiser, Clustering in real space and in redshift space, Mon. Not. R. Astron. Soc. **227**, 1 (1987).

[51] A. J. S. Hamilton, Measuring omega and the real correlation function from the redshift correlation function, Astrophys. J. **385**, L5 (1992).

[52] A. J. S. Hamilton, Linear redshift distortions: A review, arXiv:astro-ph/9708102.

[53] G. Valogiannis, R. Bean, and A. Aviles, An accurate perturbative approach to redshift space clustering of biased tracers in modified gravity, J. Cosmol. Astropart. Phys. 01 (2020) 055.

[54] K. B. Fisher, On the validity of the streaming model for the redshift-space correlation function in the linear regime, Astrophys. J. **448**, 494 (1995).

[55] B. A. Reid and M. White, Towards an accurate model of the redshift-space clustering of haloes in the quasi-linear regime, Mon. Not. R. Astron. Soc. **417**, 1913 (2011).

[56] L. Wang, B. Reid, and M. White, An analytic model for redshift-space distortions, Mon. Not. R. Astron. Soc. **437**, 588 (2014).

[57] Ya. B. Zeldovich, Gravitational instability: An approximate theory for large density perturbations, Astron. Astrophys. **5**, 84 (1970), http://adsabs.harvard.edu/full/1970A%26A.....5...84Z.

[58] T. Buchert, A class of solutions in Newtonian cosmology and the pancake theory, Astron. Astrophys. **223**, 9 (1989), https://ui.adsabs.harvard.edu/abs/1989A%26A...223....9B/abstract.

[59] F. R. Bouchet, S. Colombi, E. Hivon, and R. Juszkiewicz, Perturbative Lagrangian approach to gravitational instability, Astron. Astrophys. **296**, 575 (1995), https://ui.adsabs.harvard.edu/abs/1995A%26A...296..575B/abstract.

[60] E. Hivon, F. R. Bouchet, S. Colombi, and R. Juszkiewicz, Redshift distortions of clustering: A Lagrangian approach, Astron. Astrophys. **298**, 643 (1995), https://ui.adsabs.harvard.edu/abs/1995A%26A...298..643H/abstract.

[61] A. N. Taylor and A. J. S. Hamilton, Nonlinear cosmological power spectra in real and redshift space, Mon. Not. R. Astron. Soc. **282**, 767 (1996).

[62] T. Matsubara, Resumming cosmological perturbations via the Lagrangian picture: One-loop results in real space and in redshift space, Phys. Rev. D **77**, 063530 (2008).

[63] T. Matsubara, Nonlinear perturbation theory with halo bias and redshift-space distortions via the Lagrangian picture, Phys. Rev. D **78**, 083519 (2008); **78**, 109901(E) (2008).

[64] J. Carlson, B. Reid, and M. White, Convolution Lagrangian perturbation theory for biased tracers, Mon. Not. R. Astron. Soc. **429**, 1674 (2013).

[65] T. Matsubara, Recursive solutions of Lagrangian perturbation theory, Phys. Rev. D **92**, 023534 (2015).

[66] A. Aviles and J. L. Cervantes-Cota, Lagrangian perturbation theory for modified gravity, Phys. Rev. D **96**, 123526 (2017).

[67] A. Aviles, M. A. Rodriguez-Meza, J. De-Santiago, and J. L. Cervantes-Cota, Nonlinear evolution of initially biased tracers in modified gravity, J. Cosmol. Astropart. Phys. 11 (2018) 013.

[68] G. Valogiannis and R. Bean, Convolution lagrangian perturbation theory for biased tracers beyond general relativity, Phys. Rev. D **99**, 063526 (2019).

[69] P. Brax, C. van de Bruck, A.-C. Davis, and D. J. Shaw, f(R) gravity and Chameleon theories, Phys. Rev. D **78**, 104021 (2008).

[70] J. Khoury and A. Weltman, Chameleon cosmology, Phys. Rev. D **69**, 044026 (2004).

[71] J. Khoury and A. Weltman, Chameleon Fields: Awaiting Surprises for Tests of Gravity in Space, Phys. Rev. Lett. **93**, 171104 (2004).

[72] C. Burrage and J. Sakstein, Tests of chameleon gravity, Living Rev. Relativity **21**, 1 (2018).

[73] H. Desmond and P. G. Ferreira, Galaxy morphology rules out astrophysically interesting $f(R)$, Phys. Rev. D **102**, 104060 (2020).

[74] T. Clifton, P. G. Ferreira, A. Padilla, and C. Skordis, Modified gravity and cosmology, Phys. Rep. **513**, 1 (2012).

[75] A. Vainshtein, To the problem of nonvanishing gravitation mass, Phys. Lett. **39B**, 393 (1972).

[76] E. Babichev and C. Deffayet, An introduction to the Vainshtein mechanism, Classical Quantum Gravity **30**, 184001 (2013).

[77] K. Koyama, Ghosts in the self-accelerating universe, Classical Quantum Gravity **24**, R231 (2007).

[78] G.-B. Zhao, B. Li, and K. Koyama, N-body simulations for f(R) gravity using a Self-adaptive particle-mesh code, Phys. Rev. D **83**, 044007 (2011).

[79] G. Valogiannis and R. Bean, Efficient simulations of large-scale structure in modified gravity cosmologies with comoving Lagrangian acceleration, Phys. Rev. D **95**, 103515 (2017).

[80] A. Lewis, A. Challinor, and A. Lasenby, Efficient computation of CMB anisotropies in closed FRW models, Astrophys. J. **538**, 473 (2000).

[81] A. Lewis and S. Bridle, Cosmological parameters from CMB and other data: A Monte Carlo approach, Phys. Rev. D **66**, 103511 (2002).

[82] C. Howlett, A. Lewis, A. Hall, and A. Challinor, CMB power spectrum parameter degeneracies in the era of precision cosmology, J. Cosmol. Astropart. Phys. 04 (2012) 027.

[83] H. Winther, S. Casas, M. Baldi, K. Koyama, B. Li, L. Lombriser, and G.-B. Zhao, Emulators for the non-linear matter power spectrum beyond ΛCDM, Phys. Rev. D **100**, 123540 (2019).

[84] A. Aviles, J. L. Cervantes-Cota, and D. F. Mota, Screenings in modified gravity: A perturbative approach, Astron. Astrophys. **622**, A62 (2019).

[85] N. Kaiser, On the spatial correlations of Abell clusters, Astrophys. J. **284**, L9 (1984).

[86] G. Efstathiou, C. S. Frenk, S. D. M. White, and M. Davis, Gravitational clustering from scale-free initial conditions, Mon. Not. R. Astron. Soc. **235**, 715 (1988).

[87] V. Desjacques, D. Jeong, and F. Schmidt, Large-scale galaxy bias, Phys. Rep. **733**, 1 (2018).

[88] Z. Vlah, M. White, and A. Aviles, A Lagrangian effective field theory, J. Cosmol. Astropart. Phys. 09 (2015) 014.

[89] Z. Vlah, E. Castorina, and M. White, The Gaussian streaming model and convolution Lagrangian effective field theory, J. Cosmol. Astropart. Phys. 12 (2016) 007.

[90] R. Scoccimarro, Redshift-space distortions, pairwise velocities, and nonlinearities, Phys. Rev. D **70**, 083007 (2004).

[91] A. Font-Ribera, P. McDonald, N. Mostek, B. A. Reid, H.-J. Seo, and A. Slosar, DESI and other dark energy experiments in the era of neutrino mass measurements, J. Cosmol. Astropart. Phys. 05 (2014) 023.

[92] T. Lazeyras, C. Wagner, T. Baldauf, and F. Schmidt, Precision measurement of the local bias of dark matter halos, J. Cosmol. Astropart. Phys. 02 (2016) 018.

[93] M. White, The Zel'dovich approximation, Mon. Not. R. Astron. Soc. **439**, 3630 (2014).

[94] H. Mo and S. D. White, An Analytic model for the spatial clustering of dark matter halos, Mon. Not. R. Astron. Soc. **282**, 347 (1996).

[95] H. Mo, Y. Jing, and S. White, High-order correlations of peaks and halos: A Step toward understanding galaxy biasing, Mon. Not. R. Astron. Soc. **284**, 189 (1997).

[96] S.-F. Chen, Z. Vlah, E. Castorina, and M. White, Redshift-space distortions in lagrangian perturbation theory, J. Cosmol. Astropart. Phys. 03 (2021) 100.

[97] A. Aviles, G. Valogiannis, M. A. Rodriguez-Meza, J. L. Cervantes-Cota, B. Li, and R. Bean, Redshift space power spectrum beyond Einstein-de Sitter kernels, J. Cosmol. Astropart. Phys. 04 (2021) 039.

[98] C. Arnold, P. Fosalba, V. Springel, E. Puchwein, and L. Blot, The modified gravity light-cone simulation project—I. Statistics of matter and halo distributions, Mon. Not. R. Astron. Soc. **483**, 790 (2019).

[99] M. Davis and P. J. E. Peebles, A survey of galaxy redshifts. V—The two-point position and velocity correlations, Astrophys. J. **267**, 465 (1983).

[100] J. A. Peacock, Errors on the measurement of Ω via cosmological dipoles, Mon. Not. R. Astron. Soc. **258**, 581 (1992).

[101] S. Joudaki, P. G. Ferreira, N. A. Lima, and H. A. Winther, Testing gravity on cosmic scales: A case study of Jordan-Brans-Dicke theory, arXiv:2010.15278.

[102] N. Ramachandra, G. Valogiannis, M. Ishak, and K. Heitmann (LSST Dark Energy Science), Matter power spectrum emulator for f(R) modified gravity cosmologies, Phys. Rev. D **103**, 123525 (2021).

[103] A. Albrecht, L. Amendola, G. Bernstein, D. Clowe, D. Eisenstein, L. Guzzo, C. Hirata, D. Huterer, R. Kirshner, E. Kolb, and R. Nichol, Findings of the joint dark energy mission figure of merit science working group arXiv:0901.0721.

[104] D. Coe, Fisher matrices and confidence ellipses: A quick-start guide and software, arXiv:0906.4123.

[105] B. Bose, M. Cataneo, T. Trster, Q. Xia, C. Heymans, and L. Lombriser, On the road to per-cent accuracy IV: ReACT—computing the non-linear power spectrum beyond ΛCDM, Mon. Not. R. Astron. Soc. **498**, 4650 (2020).

[106] J. Tinker, A. V. Kravtsov, A. Klypin, K. Abazajian, M. Warren, G. Yepes, S. Gottlöber, and D. E. Holz, Toward a halo mass function for precision cosmology: The limits of universality, Astrophys. J. **688**, 709 (2008).

[107] H. A. Feldman, N. Kaiser, and J. A. Peacock, Power spectrum analysis of three-dimensional redshift surveys, Astrophys. J. **426**, 23 (1994).

[108] A. Meiksin and M. J. White, The growth of correlations in the matter power spectrum, Mon. Not. R. Astron. Soc. **308**, 1179 (1999).

[109] J. D. Cohn, Power spectrum and correlation function errors: Poisson vs. Gaussian shot noise, New Astron. **11**, 226 (2006).

[110] R. Scoccimarro, M. Zaldarriaga, and L. Hui, Power spectrum correlations induced by nonlinear clustering, Astrophys. J. **527**, 1 (1999).

[111] A. Cooray and W. Hu, Power spectrum covariance of weak gravitational lensing, Astrophys. J. **554**, 56 (2001).

[112] A. Barreira and F. Schmidt, Response approach to the matter power spectrum covariance, J. Cosmol. Astropart. Phys. 11 (2017) 051.

[113] A. J. Hamilton, C. D. Rimes, and R. Scoccimarro, On measuring the covariance matrix of the nonlinear power spectrum from simulations, Mon. Not. R. Astron. Soc. **371**, 1188 (2006).

[114] W. Hu and A. V. Kravtsov, Sample variance considerations for cluster surveys, Astrophys. J. **584**, 702 (2003).
[115] M. Takada and W. Hu, Power spectrum super-sample covariance, Phys. Rev. D **87**, 123504 (2013).
[116] Y. Li, M. Schmittfull, and U. Seljak, Galaxy power-spectrum responses and redshift-space super-sample effect, J. Cosmol. Astropart. Phys. 02 (2018) 022.
[117] A. Barreira, E. Krause, and F. Schmidt, Complete super-sample lensing covariance in the response approach, J. Cosmol. Astropart. Phys. 06 (2018) 015.
[118] Y. Li, S. Singh, B. Yu, Y. Feng, and U. Seljak, Disconnected covariance of 2-point functions in large-scale structure, J. Cosmol. Astropart. Phys. 01 (2019) 016.
[119] M. White, B. Reid, C.-H. Chuang, J. L. Tinker, C. K. McBride, F. Prada, and L. Samushia, Tests of redshift-space distortions models in configuration space for the analysis of the BOSS final data release, Mon. Not. R. Astron. Soc. **447**, 234 (2015).
[120] J. N. Grieb, A. G. Sánchez, S. Salazar-Albornoz, and C. Dalla Vecchia, Gaussian covariance matrices for anisotropic galaxy clustering measurements, Mon. Not. R. Astron. Soc. **457**, 1577 (2016).
[121] R. E. Smith, R. Scoccimarro, and R. K. Sheth, Motion of the acoustic peak in the correlation function, Phys. Rev. D **77**, 043525 (2008).